

## Phenomenological analysis of simple ion channel block in large populations of uncoupled cardiomyocytes

RADOSTIN D. SIMITEV\*, ANTESAR AL DAWOUD

*School of Mathematics & Statistics, University of Glasgow, Glasgow G12 8QQ, UK*

MUHAMAD H.N. AZIZ

*Institute of Mathematical Sciences, Universiti Malaya, 50603 K. Lumpur, Malaysia*

RACHEL MYLES AND GODFREY L. SMITH

*Institute of Cardiovascular & Medical Sciences, University of Glasgow, Glasgow G12 8TA UK*

Current understanding of arrhythmia mechanisms and design of anti-arrhythmic drug therapies hinges on the assumption that myocytes from the same region of a single heart have similar, if not identical, action potential waveforms and drug responses. On the contrary, recent experiments reveal significant heterogeneity in uncoupled healthy myocytes both from different hearts as well as from identical regions within a single heart. In this work, a methodology is developed for quantifying the individual electrophysiological properties of large numbers of uncoupled cardiomyocytes under ion channel block in terms of the parameters values of a conceptual fast-slow model of electrical excitability. The approach is applied to a population of nearly 500 rabbit ventricular myocytes for which action potential duration (APD) before and after the application of the drug nifedipine was experimentally measured (Lachaud et al., 2022, *Cardiovasc. Res.*). To this end, drug action is represented by a multiplicative factor to an effective ion conductance, a closed form asymptotic expression for APD is derived and inverted to determine model parameters as functions of APD and  $\Delta$ APD (drug-induced change in APD) for each myocyte. Two free protocol-related quantities are calibrated to experiment using an adaptive-domain procedure based on an original assumption of optimal excitability. The explicit APD expression and the resulting set of model parameter values allow (a) direct evaluation of conditions necessary to maintain fixed APD or  $\Delta$ APD, (b) predictions of the proportion of cells remaining excitable after drug application, (c) predictions of stimulus period dependency and (d) predictions of dose-response curves, the latter being in agreement with additional experimental data.

*Keywords:* asymptotics of cellular electrical excitability, action potential duration, drug response

### 1. Introduction

The heart pumps blood due to coordinated contraction of approximately 50 million of individual cardiac cells. Contraction of each myocyte is triggered by the excitation of electrical impulses known as transmembrane action potentials (AP), e.g. (Bers, 2001). When disease, inherited disorders or environmental factors prolong or shorten the duration of the action potential the heart becomes vulnerable to arrhythmias, electrical instabilities, that may rapidly deteriorate to cause fatal deficiency in cardiac output (Anumonwo & Pandit, 2015; Tse, 2016). Thus, there is strong impetus to develop anti-arrhythmic drugs that can control action potential duration and restore it to norm (Darbar, 2018). The action potential duration (APD) and its change under drug action ( $\Delta$ APD) are, therefore, primary biomarkers used to guide the design of anti-arrhythmic drugs and quantify their pharmacodynamics (Corrias et al., 2010).

\*Corresponding author. Email: [Radostin.Simitev@glasgow.ac.uk](mailto:Radostin.Simitev@glasgow.ac.uk). OrcID: [orcid.org/0000-0002-2207-5789](https://orcid.org/0000-0002-2207-5789).

Novel optics-based techniques in cardiac electrophysiology have now made it possible to design high-throughput systems capable of measuring APD and other secondary AP waveform biomarkers at rates of up to 200 cells/hr (Warren et al., 2010; Lachaud et al., 2018; Müllenbroich et al., 2021). In our recent study (Lachaud et al., 2022), AP characteristics of nearly 500 uncoupled cardiomyocytes were measured using voltage-sensitive fluorescent dyes. The cells were isolated from well-defined regions of the left ventricular wall of 12 rabbit hearts and APD values were taken from the same cells before and after specific ion channel inhibition with two different drugs. An unexpectedly large variability in the values of the action potential duration at 90% repolarization (APD<sub>90</sub>) of the uncoupled healthy cardiomyocytes was measured before the addition of the drugs. Specifically, at stimulation rate of 2 Hz the inter-quartile range of APD<sub>90</sub> was 40 to 50 ms with median value of 250 ms. This variation was not due to cell dissociation damage and it is considerably larger than regional endo-epicardial and apical-basal differences in median APD<sub>90</sub> from single hearts, as well as larger than differences in median APD<sub>90</sub> measured between the individual hearts. Measurements after inhibition of the IK(r) ionic current by 30 nM of dofetilide and after inhibition of the ICa(L) current by 1  $\mu$ M of nifedipine both showed that individual cells with near identical baseline values of APD<sub>90</sub> produce a wide range of different  $\Delta$ APD<sub>90</sub> values. The latter result demonstrates starkly that APD alone does not characterise or uniquely determine the electrophysiological response of myocytes to drugs, as often assumed. Measurements of additional, mutually-independent biomarkers are required increase the accuracy of  $\Delta$ APD<sub>90</sub> estimation irrespective of whether a data-driven or physics/physiology-based approach is employed. It is the goal of our work to interpret these findings in the light of a conceptual mathematical model as discussed next.

To understand this significant intrinsic variability, action potential waveforms, which are of ionic origin (Pandit, 2018), must be related to their underlying electrophysiological characteristics, including the conductances and kinetic parameters of the ion channels, exchangers and pumps of each individual myocyte. However, high-throughput patch-clamping of ionic currents in large numbers of cells (more than 100) are currently not feasible, and clamping myocytes already used with voltage-fluorescent dyes is an even bigger technical challenge. Mathematical ionic-current models of the AP waveform provide a valuable alternative (Clayton et al., 2011; Davies et al., 2016; Clayton et al., 2020). Following (Gemell et al., 2016; Muszkiewicz et al., 2016), a rejection sampling procedure was used in (Lachaud et al., 2022) for this purpose. The modelling procedure consisted of (a) selecting the detailed ionic current model of Shannon et al. (2004) as a mathematical representation of the rabbit myocytes, (b) a parameter sensitivity analysis to determine the ionic conductances in the model that most strongly affecting the AP waveform followed by (c) their random variation to generate a model 50,000 variants, and finally (d) a calibration of the ensemble by rejecting model variants that fell outside the ranges and the histogram distribution of the experimentally measured APD<sub>90</sub> values. However, the Shannon et al. (2004) model variants calibrated in this way were not cell-specific, the population was not unique and less sensitive parameters remained at baseline values, for reasons outlined below.

While offering valuable insight and being routinely employed to interpret experimental findings, extrapolate animal data to human system context and test novel hypotheses, detailed ionic models such as that of Shannon et al. (2004) are prohibitively complicated (Sigg et al., 2010). For example, the latter model consists of 45 ordinary differential equations and includes 177 model parameters. Many of these parameters and equations are poorly constrained, some even redundant, because such models are typically developed by extending and re-using components from earlier models, as advocated by large international initiatives like the Physiome Project (Bassingthwaite, 2000) and the CellML Project (Miller et al., 2010). For instance, the modern human ventricular models of ten Tusscher et al. (2004) and Iyer et al. (2004) include parameters inherited from studies in at least 9 different species over a range of 6 different temperatures (Niederer et al., 2009), and this is likely true for the model of Shannon

et al. (2004), as well. Despite intensive research effort expended to estimate their parameter uncertainty (Clayton et al., 2020), calibrate models to identifiable and reliable experimental protocols (Whittaker et al., 2020; Clerx et al., 2019) and increase their reproducibility (Cooper et al., 2016; Johnstone et al., 2016), detailed cardiac cell models remain difficult to adapt to situations to which they have not been fitted (Wilhelms et al., 2013). Most importantly, detailed cardiac models are becoming increasingly difficult for causal inference (Biktashev et al., 2008a), as also evidenced by the need to resort to rejection sampling procedures such as described above in relation to the analysis of the data of Lachaud et al. (2022).

With this motivation, the aim of our study is to employ a simple phenomenological model of the transmembrane action potential in order to formulate a mathematical description of the experimental procedure of Lachaud et al. (2022). A variety of simplified phenomenological models of the cardiac action potential exist (FitzHugh, 1961; Nagumo et al., 1962; Aliev & Panfilov, 1996; Mitchell, 2003), to list a few. The model of McKean (1970), featuring piece-wise linear kinetics and only three intrinsic parameters will be used here, being arguably the simplest such model. The McKean (1970) equations allow exact solution for the action potential waveform in closed form. Here, a phase-space analysis will be used to derive an even simpler invertible asymptotic relationship between APD and the parameters of the model with the goal of illustrating explicitly the geometric behaviour of these quantities. A natural calibration of the model to the experimental data of (Lachaud et al., 2022) will be proposed that will allow to determine uniquely the individualised values of the McKean (1970) model parameters corresponding to each rabbit myocyte used in experiments. Admittedly, the McKean (1970) model and its parameters have no direct correspondence to myocyte electrophysiological structures and processes such as ion channel conductances and kinetic parameters of transmembrane currents. However, the analysis is valuable as it provides an mathematically well-defined test case that can be used to conceptualise experiments and validate other parameter inference and data-driven approaches such as rejection sampling and calibration (Muszkiewicz et al., 2016; Gemmell et al., 2016; Whittaker et al., 2020), inverse regression (Sobie, 2009; Sarkar & Sobie, 2010), machine learning (Feeny et al., 2020; Trayanova et al., 2021), Gaussian and Bayesian emulation (Coveney & Clayton, 2020; Coveney et al., 2021) and multi-objective optimisation (Pouranbarani et al., 2019) of detailed ionic AP models.

For completeness, we mention data-driven models as an alternative strategy for studying the intrinsic variability of action potential waveforms. A data-driven model is a statistical model for prediction of a target quantity as a function of observed features without recourse to an intermediate “first-principles” model. Examples include regression and neural-network models; Hastie et al. (2009) provides an extensive general overview while specific applications of data-driven approaches to cardiac cellular excitability were already cited above. Typically, data-driven models are relatively accurate but are less interpretable, computationally efficient and generalizable than physics/physiology-based models. The development of purely data-driven approaches is at present limited by experimental factors. For instance, measurements of  $\text{Trise}$ ,  $\text{APD}_{50}$ ,  $\text{APD}_{30}$ , and triangulation index are also reported in (Lachaud et al., 2022), but the uncertainty in measuring  $\text{TRise}$  is significant, while biomarkers  $\text{APD}_{XX}$  are strongly correlated with each other.

## 2. Asymptotic approximation of APD in the McKean model

### 2.1 The McKean equations

To interpret the results of Lachaud et al. (2022), we consider, as a phenomenological model of the action potential of uncoupled rabbit ventricular myocytes, the following planar system of first-order ordinary

differential equations

$$\frac{dv}{dt} = \varepsilon^{-1} f(v, w; a, b), \quad f(v, w; a, b) := -(v - H(v - a) + w), \quad (2.1a)$$

$$\frac{dw}{dt} = g(v, w; a, b), \quad g(v, w; a, b) := v - bw. \quad (2.1b)$$

Here  $v$  and  $w$  are dynamical variables of time  $t$ , interpreted as the myocyte trans-sarcolemmal voltage potential and an effective gating variable, respectively,  $H(x)$  denotes the Heaviside step function, and  $a$ ,  $b$  and  $\varepsilon$  are model parameters with  $0 < \varepsilon \ll 1$ . In the experiments of [Lachaud et al. \(2022\)](#), myocytes were stimulated at 2 Hz using a 2 ms duration voltage pulse at 1.5 threshold via carbon electrodes. To mimic this stimulation protocol, we complement equations (2.1) by the initial conditions

$$v(0) = v_{\text{stim}} > a, \quad w(0) = w_0, \quad (2.2a)$$

and then advance via a sequence of initial value problems on time intervals  $t \in (k\beta, (k+1)\beta]$ ,  $k \in \mathbb{N}$  with duration  $\beta$  (basic cycle length, BCL), each with initial conditions

$$v(k\beta) = v_{\text{stim}}, \quad w(k\beta) = w((k-1)\beta) = w_\beta. \quad (2.2b)$$

The statement that  $w(k\beta) = w((k-1)\beta) = w_\beta$  for some  $k > m$  will be justified in subsection 2.4, below.

Equations (2.1) were proposed by [McKean \(1970\)](#) as a model of the action potential of spiking neurons. They are qualitatively equivalent to the FitzHugh-Nagumo equations ([FitzHugh, 1961](#); [Nagumo et al., 1962](#)), the latter being in turn a reduction of the pioneering [Hodgkin & Huxley \(1952\)](#) model of the action potentials in the squid giant axon. These equations been extensively studied in the literature e.g. ([Rinzel & Keller, 1973](#); [Wang, 1988a,b](#); [Tonnelier, 2003](#); [Bezekci et al., 2015](#)) and below we recall, briefly and informally, some elements of their geometric singular perturbation analysis with the aim of determining (a) the parameter range where the model is excitable, and (b) an asymptotic expression for the APD, both necessary for modelling of experimental results in subsequent sections.

## 2.2 Phase portrait

The solutions to the [McKean \(1970\)](#) model have a generic action potential waveform as shown in Figure 1(a), c.f. figure 1 and 2 of ([Lachaud et al., 2022](#)) for comparison to waveforms measured in experiments. To understand these solutions we consider the singular asymptotic limit  $\varepsilon \rightarrow 0^+$  in which equations (2.1) reduce to a fast-time subsystem

$$\frac{dv}{d\tau} = f(v, w), \quad \frac{dw}{d\tau} = 0, \quad (2.3)$$

when written in terms of the “fast” time variable  $\tau := \varepsilon^{-1}t$ , and to a slow-time subsystem

$$0 = f(v, w), \quad \frac{dw}{dt} = g(v, w), \quad (2.4)$$

when written in terms of the original “slow” time variable  $t = O(1)$ . The nullcline  $f(v, w) = 0$  plays a special role in both systems (2.3) and (2.4), and it is known as the “critical set” or the “reduced slow set” of (2.1), because it is in one-to-one correspondence to fixed points of the fast subsystem (2.3), and because the trajectories of the slow subsystem (2.4) are constrained to follow it. The critical set,  $f(v, w) =$

0, is a piece-wise linear caricature of a cubic function of  $v$  as illustrated in Figure 1(b). Specifically, it has local minima and maxima at the points  $M_{\min} = (a, -a)$  and  $M_{\max} = (a, 1-a)$ , respectively, and roots

$$\begin{cases} v_{\text{sys}} = 1 - w & \text{for } w \in (-\infty, -a], \\ v_{\text{dia}} = -w, \quad v_{\text{thr}} = a, \quad v_{\text{sys}} = 1 - w & \text{for } w \in [-a, 1-a], \\ v_{\text{dia}} = -w & \text{for } w \in [1-a, \infty). \end{cases} \quad (2.5)$$

Since  $f(v, w) < 0$  in the region  $\Omega_f^- := \{(v, w) \in \mathbb{R}^2 : w > \bar{w} \text{ where } f(v, \bar{w}) = 0\}$ , and  $f(v, w) > 0$  in the region  $\Omega_f^+ := \{(v, w) \in \mathbb{R}^2 : w < \bar{w} \text{ where } f(v, \bar{w}) = 0\}$ , the branches  $v_{\text{sys}}(w)$  and  $v_{\text{dia}}(w)$ , called ‘‘systolic’’ and ‘‘diastolic’’ respectively, consist of stable attracting fixed points and the ‘‘threshold’’ branch  $v_{\text{thr}}(w)$  consists of unstable repelling fixed points of the fast-subsystem (2.3). The second nullcline  $g(v, w) = 0$  is a straight line which partitions the phase plane in two regions  $\Omega_g^- := \{(v, w) \in \mathbb{R}^2 : w > \bar{w} \text{ where } g(v, \bar{w}) = 0\}$  where  $g(v, w) < 0$ , and  $\Omega_g^+ := \{(v, w) \in \mathbb{R}^2 : w < \bar{w} \text{ where } g(v, \bar{w}) = 0\}$  where  $g(v, w) > 0$  and thus determines the direction of the slow flow of (2.3) along the critical set. These facts are illustrated by the vector field shown in Figure 1(b). Thus, in the singular approximations given by (2.3) and (2.4) a typical trajectory of the McKean model (2.1) consists of fast jumps to one of the attracting branches of the critical set followed by slow motions to the end the attracting region or until a globally stable fixed point is reached as illustrated in Figure 1(b). Global fixed points occur at the intersection of the two nullclines and apart from degenerate cases there exists either one single or three distinct fixed points given by

$$(v_*, w_*) \in \begin{cases} \{(0, 0)\} & \text{if } b < a/(1-a), \\ \{(0, 0), (a, a/b), (b/(1+b), 1/(1+b))\} & \text{if } b \geq a/(1-a). \end{cases} \quad (2.6)$$

### 2.3 Asymptotic approximation of excitability

Biological excitability is usually described as a reaction of a system to an external stimulus that invokes a sufficiently large finite response before return to a unique global equilibrium. It follows that in McKean’s model (2.1), excitability corresponds to the case of a single stable attractor located between the fold points  $M_{\min}$  and  $M_{\max}$  on the diastolic branch  $v_{\text{sys}}(w)$  and hence to a parameter space given by

$$\Omega_{\text{ex}} = \{(a, b) \in \mathbb{R}^2 : b > -1 \cap b < a/(1-a) \cap a > 0 \cap a < 1\}. \quad (2.7)$$

Region  $\Omega_{\text{ex}}$  is visualised in Figure 2(a). Indeed, in this case starting from the initial conditions (2.2b), a trajectory performs a fast jump of infinitesimally short duration  $O(\varepsilon)$  from point  $(v_{\text{stim}}, w_\beta)$  to point  $(v_{\text{sys}}(w_\beta), w_\beta)$  governed by the fast subsystem (2.3). Next, it follow the systolic branch from the latter point to point  $M_{\max}$  for a period of duration found by integrating the slow subsystem (2.4),

$$\alpha := \int_{w_\beta}^{1-a} dt = \int_{w_\beta}^{1-a} \frac{dw}{g(v_{\text{sys}}(w), w)} = \frac{1}{1+b} \log \left( \frac{1 - (1+b)w_\beta}{1 - (1+b)(1-a)} \right). \quad (2.8)$$

At the fold point  $M_{\max}$  the systolic branch of the critical set  $v_{\text{sys}}$  terminates and switches to the repelling threshold branch  $v_{\text{thr}}$  so the trajectory makes another infinitesimally short fast jump over to point  $(v_{\text{dia}}(1-a), 1-a)$ . Finally, the trajectory follows the attracting diastolic branch  $v_{\text{dia}}(w)$  towards the single global stable fixed point  $(0, 0)$  for period of duration found by integrating the slow subsystem (2.4),

$$\delta := \int_{1-a}^{w_\beta} dt = \int_{1-a}^{w_\beta} \frac{dw}{g(v_{\text{dia}}(w), w)} = \frac{1}{1+b} \log \left( \frac{1-a}{w_\beta} \right), \quad (2.9)$$

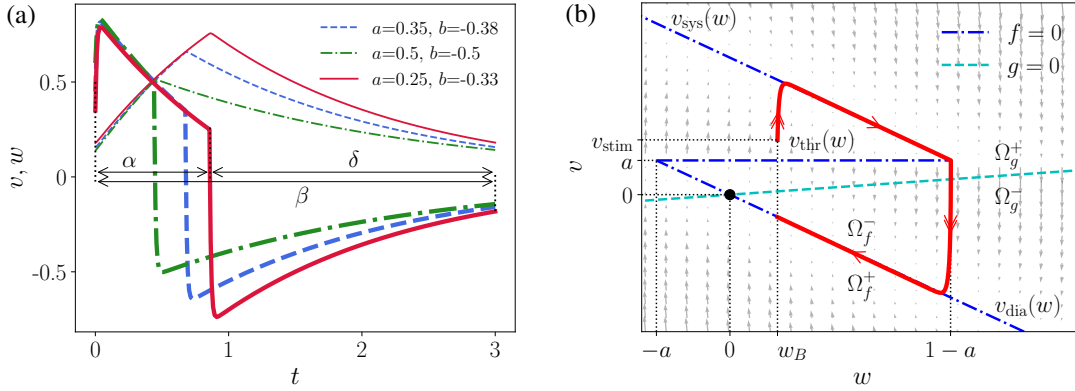


FIG. 1: (a) Three examples of action potential solutions to the McKean equations (2.1). The “voltage”  $v(t)$  (thick curves) and the effective “gating variable”  $w(t)$  (thin curves) are shown as functions of time for parameter values  $\varepsilon = 0.01$ ,  $\beta = 3$  and randomly selected combinations of  $a$  and  $b$  as shown in the legend. The action potential duration  $\alpha$ , diastolic interval  $\delta$ , and basic cycle length  $\beta$  are annotated on one of the AP curves. (b) Phase portrait and vector field of the McKean equations (2.1) and associated notation. The nullclines  $f = 0$  and  $g = 0$  are shown as a dash-dotted blue line and a dashed turquoise line, respectively. The single attracting global equilibrium  $(0, 0)$  is marked with a black dot marker. A typical trajectory is shown in a solid red line where a double arrow indicates a fast piece and a single arrow indicates a slow piece of the trajectory. Parameter values used are  $a = 0.25$ ,  $b = 0.3$ ,  $\varepsilon = 0.01$  and correspond to excitable dynamics.

when it receives its next excitation stimulus at  $(v_{\text{stim}}, w_\beta)$  and repeats these motions as illustrated in Figure 1(b). Our presentation has been rather informal, so we remark that the asymptotic analysis of fast-slow systems, such as the McKean model (2.1), has a rigorous foundation grounded in classical theorems due to Tikhonov (1952); Pontryagin (1957); Fenichel (1979) and a good exposition with an extensive list of references may be found in (Kuehn, 2015).

#### 2.4 APD restitution under periodic stimulation

So far, we have not discussed the parameter  $w_\beta$  introduced in the initial conditions (2.2b). In fact, this is not an independent parameter, rather it is determined by the prescribed basic cycle length  $\beta$ . Conditions for uniqueness and existence of solutions to an initial-value problem require that for the solutions of equations (2.1) to be identical up to a time shift (i.e. periodic APs) on two consecutive time intervals  $t \in (k\beta, (k+1)\beta]$ ,  $k \in \mathbb{N}$ , they must start from identical initial conditions. This implies that a periodic train of action potentials exists only when the sequence  $\{w(k\beta), k = 0, 1, \dots\}$  converges to a unique value  $w_\beta$ , possibly after a transient period of a finite number of stimuli  $k > m$ . There may exist parameter values including that of  $\beta$ , for which the sequence does not converge but generates more complex behaviour such as alternans. Alternans, (more precisely, APD alternans, as other types also exist) is a regime of myocyte response to periodic stimulation where action potentials alternate in duration between long and short even though the pacing cycle length remains constant, see e.g. (Qu et al., 2014). However, investigating these possibilities is beyond the scope of the current analysis, and here we assume a strictly periodic response to the external stimulation. Under this assumption and proceeding to

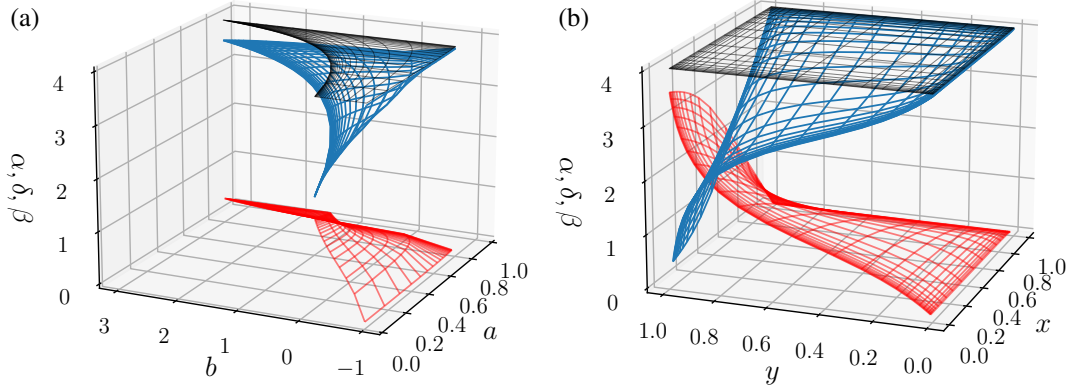


FIG. 2: Asymptotic expressions (2.12a) and (2.12b) for the action potential duration  $\alpha$  (red wire-frame) and diastolic interval  $\delta$  (blue wire-frame), respectively, (a) as functions of the McKean model parameters  $a$  and  $b$  and (b) as functions of the “rectangular” variables  $x$  and  $y$  defined in equation (2.13). The value of the basic cycle length is  $\beta = 4$  and the surfaces  $\beta = \alpha + \delta$  (black wire-frame) are plotted as a test and to illustrate the parameter space  $\Omega_{\text{ex}}$  for excitable dynamics given by (2.7).

employ asymptotic approximation, we neglect the duration of any fast jumps as being of order  $O(\varepsilon)$  and identify expression (2.8) as the duration of the action potential, APD, and expression (2.9) as its diastolic interval, DI. Thus, we require, that the sum of the APD and the DI equals the BCL,

$$\beta = \alpha + \delta = \frac{1}{1+b} \log \left( \frac{(1 - (1+b)w_\beta)(1-a)}{(1 - (1+b)(1-a))w_\beta} \right). \quad (2.10)$$

Solving this algebraic equation yields the value of  $w_\beta$  necessary to establish a periodic train of APs,

$$w_\beta = \left( (1+b) + \exp((1+b)\beta) (1 - (1+b)(1-a)) / (1-a) \right)^{-1}. \quad (2.11)$$

Substituting (2.11) into (2.8), we arrive at an explicit closed form expressions for the APD and the DI as functions of the intrinsic model parameters  $a$  and  $b$  and the protocol dependent basic cycle length parameter  $\beta$ ,

$$\alpha(a, b, \beta) = \frac{1}{\tilde{b}} \log \left( \frac{\exp(\tilde{b}\beta)}{\tilde{a}\tilde{b} + (1 - \tilde{a}\tilde{b}) \exp(\tilde{b}\beta)} \right), \quad \tilde{a} := 1 - a, \quad \tilde{b} := 1 + b, \quad (2.12a)$$

$$\delta(a, b, \beta) = \beta - \alpha(a, b, \beta), \quad (2.12b)$$

with  $\tilde{a}$  and  $\tilde{b}$  introduced for brevity only. These expressions along with equation (2.10) are illustrated in Figure 2 as surfaces over the parameter region of excitable dynamics,  $\Omega_{\text{ex}}$ . The outline of  $\Omega_{\text{ex}}$  seen in Figure 2(a) and illustrates the fact that one of its boundaries,  $a = 1$ , is an asymptote to another,

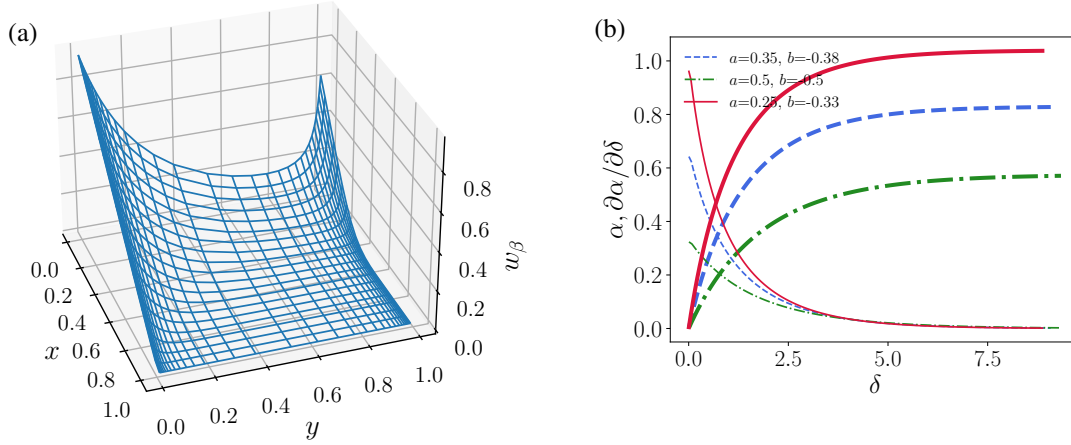


FIG. 3: (a) The initial condition  $w_\beta$  required for conformance to stimulation with fixed period  $\beta = 4$  given by equation (2.11) as a function of the “rectangular” variables  $x$  and  $y$  defined in (2.13). (b) Examples of asymptotic restitution curves  $\alpha$  as a function of  $\delta$  (thick lines) and their derivatives  $\partial_\delta \alpha$  (thin lines) for selected McKean parameter values given in the legend.

$b = a/(1 - a)$ . This makes visualisation of results in the  $(a, b)$  parameter plane difficult and we introduce a change of variables

$$a = x, \quad b = y/(1 - x) - 1, \quad x \in (0, 1), \quad y \in (0, 1), \quad (2.13)$$

that maps  $\Omega_{\text{ex}}$  into the rectangular domain  $(x, y) \in (0, 1) \times (0, 1)$ . The result is illustrated in Figure 2(b) which is identical to Figure 2(a) but uses  $x$  and  $y$  as independent variables. We remark that for fixed values of the parameters  $a$  and  $b$ , the relation between APD and DI is known as the restitution curve and is widely used in physiological experiments to infer the stability of periodic AP trains from the condition that alternans occur for values of  $\delta$  for which the slope of the restitution curve is greater than unity, i.e.  $|\partial_\delta \alpha| > 1$ , see e.g. (Qu et al., 2014) and references within. An asymptotic restitution curve for the McKean model can be obtained in parametric form from expressions (2.12a) and (2.12b) as  $(\delta(a, b, \beta), \alpha(a, b, \beta))$  with the basic cycle length  $\beta$  taking the role of the parameter along the curve. Restitution curves and their gradients are plotted in Figure 3(b) for several randomly selected combinations of parameter values  $a$  and  $b$  and show the generic shape known from experimental measurements with the slope indicating that instabilities do not occur at these parameter values.

Figure 3(a) shows the value of  $w_\beta$  found from expression (2.11) as a function of the parameters  $a$  and  $b$  at a fixed basic cycle length  $\beta$ . The figure illustrates a fact that is perhaps insufficiently appreciated. Each model in a population of uncoupled non-identical McKean models is characterised by different values of  $a$  and  $b$ . Thus, each model requires a different value of  $w_\beta$  to produce a stable periodic response to a common pacing sequence. Since  $w_\beta$  is the value of the effective gating variable at the moment of stimulation, and channel blocking drugs seek to alter the proportion of open channels, individual myocytes will be affected to a different extent by a drug dosage common to all cells.

We remark that several other variants of the McKean kinetics have been proposed e.g. (McKean, 1970; Barkley, 1991; Fall et al., 2004) and along with the FitzHugh-Nagumo model these would yield



qualitatively equivalent results, even though not in the convenient closed form found here. Finally and most importantly, we note that the McKean equations (2.1) are an appropriate phenomenological model of the rabbit ventricular APD restitution because the archetypal asymptotic structure of realistic cardiac AP models includes a conventional Tikhonov slow-time subsystem of McKean type even though it is essentially non-Tikhonov overall as demonstrated by [Biktashev et al. \(2008b\)](#).

### 3. Application of McKean asymptotics to ion-channel block experiments

#### 3.1 Model of drug action

We now proceed to apply the asymptotic results obtained in the preceding section to the ion-channel block experiments of [Lachaud et al. \(2022\)](#). In these experiments over 500 myocytes were isolated from rabbit left ventricular walls and significant cell-to-cell variability in APD was established for the first time. Although cells were extracted from different apical/basal and endo/mid/epicardial sub-regions of 12 different animal hearts, we will treat them here as a single large and diverse myocyte population. The myocytes were loaded with a voltage-sensitive dye and subjected to a periodic excitation stimulus with basic cycle length 500 ms (i.e. experimental stimulation frequency of 2 Hz). In a second stage of the experiment, 1  $\mu\text{M}$  of the drug nifedipine was applied to cells to examine their response to ion channel blocking drugs. Fluorescence signals were recorded from all cells both before and after drug application and selected AP waveform biomarkers, principally the action potential duration  $\text{APD}_{90}$ , were measured for every cell able to follow the stimulation protocol for more than 4 min. Detailed description of the experimental methods, quality control protocols along with descriptive statistics of sub-populations, estimates of experimental error, and experimental datasets can be found in ([Lachaud et al., 2022](#)).

We assume that myocytes can be described mathematically by the McKean equations (2.1). Let

$$\mathcal{D}(B, \Gamma) = \left\{ \left( A_i(B), (A_i(B) + \Delta A_i(B, \Gamma)) \right), \quad i = 1, \dots, N \right\} \quad (3.1)$$

be a set of experimental data points consisting of pairs of action potential duration values measured before and after drug application,  $A_i$  and  $(A_i + \Delta A_i)$  respectively, for each cell  $i = 1, \dots, N$ , at a fixed experimental basic cycle length  $B$  and drug concentration  $\Gamma$ . Here,  $B = 500$  ms,  $\Gamma = 1$   $\mu\text{M}$  nif., and  $N = 496$ . Let

$$\mathcal{P}(\beta, \gamma) = \left\{ (a_i, b_i), \quad i = 1, \dots, N \right\} \quad (3.2)$$

be a set of corresponding McKean model parameter pairs  $a_i$  and  $b_i$  to be determined for each cell  $i$ . We relate the action potential duration values before and after drug application to the McKean model parameters by the following set of  $2N$  non-linear equations

$$A_i/B = \alpha(a_i, b_i, \beta)/\beta, \quad (3.3a)$$

$$(A_i + \Delta A_i)/B = \alpha(\gamma a_i, b_i, \beta)/\beta, \quad i = 1, \dots, N, \quad (3.3b)$$

where  $\alpha(\cdot)$  is the asymptotic expression (2.12a) for the action potential duration,  $\beta$  is the value of the basic cycle length, and  $\gamma > 0$  is a parameter representing drug action in the McKean model, respectively. Since myocytes are uncoupled in the experiment, these  $2N$  equations decouple to a set of  $N$  independent pairs of equations one per each cell, and for brevity, subscripts  $i$  will be used only to denote specific cell values and omitted when discussion is valid for any arbitrary cell. Drug action is encoded in equations (3.3b) by introducing the multiplicative factor  $\gamma$  in front of the parameter  $a$ . Indeed, even though

the McKean model has no relation to realistic electrophysiological processes and structures in the cardiomyocytes, the parameter  $a$  plays a role similar to that of a channel current conductance: it is the only parameter on the right-hand side of the McKean “voltage” equation (2.1a), which in turn represents the total sum of all ionic currents in physiologically-realistic models. The second McKean parameter  $b$  controls the rate of change of the effective gating variable  $w$  via equation (2.1b), and so must be interpreted as an effective kinetic parameter. In the following, we will further restrict the attention to the case of  $\gamma > 1$  to compare with available nifedipine data. Note, that  $\gamma > 1$  does not mean that ion channels are enhanced but only that the  $v$ -nullcline is translated up the  $v$ -axis. Finally, the factor  $B/\beta$  is introduced to convert experimental and model APD values,  $A$  and  $\alpha$ , which are measured in different units, to a common non-dimensional form by scaling these with the experimental and model cycle lengths  $B$  and  $\beta$ , respectively.

Dofetilide data is also reported in (Lachaud et al., 2022) but will not be modelled here. Dofetilide has a more complex effect: it prolongs the APD of some cells while simultaneously shortening the APD of other cells, see Figure 3B(iii) of (Lachaud et al., 2022). Crumb et al. (2016) and Li et al. (2017) suggest that dofetilide is a multi-channel blocker that acts on several distinct ion channels. So considering the case  $\gamma < 1$ , that only prolongs APD, is insufficient to capture the effect of this drug. To model the effect of dofetilide two distinct “effective conductance” parameters like  $a$  are required, one of which shortens and the second of which prolongs the APD, so that in combination they reproduce the measured response to dofetilide. However, only one such parameter,  $a$ , is present in McKean’s model. The second McKean parameter,  $b$ , is an effective kinetic parameter and cannot be used for this purpose.

The multiplicative model  $\bar{a} = \gamma a$ , where  $a$  and  $\bar{a}$  are the values of the McKean parameter  $a$  before and after drug administration, arises as a linearisation of the general relation  $\bar{a} = \bar{a}(\Gamma)$  of the parameter  $a$  as a function of the drug concentration  $\Gamma$ . Indeed, for sufficiently small drug concentration values

$$\bar{a} = \bar{a}(\Gamma) \approx (1 + k\Gamma)a, \quad a = \bar{a}(0), \quad k = \frac{\partial \bar{a}}{\partial \Gamma}(0),$$

so that the multiplication factor  $\gamma$  depends linearly on the drug concentration

$$\gamma := (1 + k\Gamma).$$

The constant  $k$  can be eliminated using a suitable calibration  $\gamma^* = (1 + k\Gamma^*)$ , so that an explicit relation between the drug concentration  $\Gamma$  and the drug action parameter  $\gamma$  can be found,

$$\Gamma = \Gamma^* \frac{\gamma - 1}{\gamma^* - 1}.$$

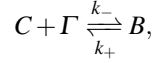
This result is used in equation (4.1) while calibration values  $\gamma^*$  and  $\Gamma^*$  are discussed in section 3.3 below. Our multiplicative model bears similarity to the so called “conductance-block” model of drug action widely used with realistic cardiac ionic current models. In realistic models an ion channel current takes the form

$$I_j = g_j^0 O(V - E_j),$$

where,  $g_j^0$  is the maximal conductance of a population of fully open channels of type  $j$ ,  $O$  is its open probability, and  $E_j$  is the reversal potential for the species of ion which flows through these channels. To account for drug action the maximal conductance  $g_j$  is multiplied by the factor

$$\gamma_{\text{ion}} = K_d / (K_d + \Gamma),$$

representing the percentage  $C/C_0$  of channels  $C$  remaining unbound in the presence of the drug. The latter expression is obtained from a steady-state approximation of the law of mass action for the reaction



where  $k_{\pm}$  are reaction rates,  $C$  and  $B$  are open and bound channels with  $C + B = C_0$  being the entire channel population, e.g. (Keener & Sneyd, 2009). The equilibrium constant  $K_d := k_-/k_+$  measures the potency of the drug and is often approximated by the half-maximal inhibitory concentration (IC50) measured in experiments. The ‘conductance-block’ formulation is widely used in numerical studies (Brennan et al., 2009; Mirams et al., 2011), but it cannot be applied directly here as the McKean parameter  $a$  is not an ion channel conductance even though it effectively plays the role of one.

### 3.2 Domain and existence of solutions

It is important to note that equations (3.3) are defined only on a subset of the full domain of excitability  $\Omega_{\text{ex}}^{\gamma} \subset \Omega_{\text{ex}}$  where  $\Omega_{\text{ex}}$  is given by (2.7). Indeed, for a cell to remain excitable after drug application the values of the parameter  $a$  must be restricted to the shorter interval  $a \in (0, 1/\gamma)$  rather than to the interval  $(0, 1)$ , because after drug application the effective conductance is  $\bar{a} = \gamma a$  and a necessary condition for equation (2.12a) to be valid is  $\bar{a} < 1$ . Therefore, equations (3.3) are restricted to the domain

$$\Omega_{\text{ex}}^{\gamma} = \left\{ (a, b) \in \mathbb{R}^2 : b > -1 \cap b < a/(1-a) \cap a > 0 \cap a < 1/\gamma \right\}. \quad (3.4)$$

The domain is visualised in Figures 4(a) and 5(b).

We now clarify the conditions for existence of solutions to equations (3.3). As noted, this system of  $2N$  nonlinear algebraic equations decouples to a set of  $N$  independent pairs one per each cell, and we consider one such pair of equations in the symbolic form

$$\mathbf{F}(A, \Delta A, a, b) = \mathbf{0}, \quad (3.5a)$$

where  $\mathbf{F} : S \subset \mathbb{R}^4 \rightarrow \mathbb{R}^2$  is a vector-valued continuous function with components  $F_1$  and  $F_2$  given by

$$\mathbf{F} = \begin{pmatrix} F_1 \\ F_2 \end{pmatrix} = \begin{pmatrix} A/B - \alpha(a, b, \beta)/\beta \\ (A + \Delta A)/B - \alpha(\gamma a, b, \beta)/\beta \end{pmatrix}. \quad (3.5b)$$

We write the points in  $\mathbb{R}^4$  in the form  $(\mathbf{x}, \mathbf{y})$  where  $\mathbf{x} = (A, \Delta A) \in \mathbb{R}^2$  and  $\mathbf{y} = (a, b) \in \mathbb{R}^2$  and recall that, by the implicit function theorem, if  $(\mathbf{x}_0, \mathbf{y}_0) \in S$  is a point such that

$$\mathbf{F}(\mathbf{x}_0, \mathbf{y}_0) = \mathbf{0} \quad \text{and} \quad \det [\partial_{\mathbf{y}} \mathbf{F}]_{(\mathbf{x}_0, \mathbf{y}_0)} \neq 0, \quad (3.6)$$

then for every  $\mathbf{x}$  in some neighbourhood of  $\mathbf{x}_0$  there exist a unique function with a value  $\mathbf{y} = \mathbf{f}(\mathbf{x})$  in some neighbourhood of  $\mathbf{y}_0$  such that  $\mathbf{F}(\mathbf{x}, \mathbf{y} = \mathbf{f}(\mathbf{x})) = \mathbf{0}$ . Here,

$$\det [\partial_{\mathbf{y}} \mathbf{F}] = J = \det \left( \frac{\partial (F_1, F_2)}{\partial (a, b)} \right) \quad (3.7)$$

is the determinant of the Jacobian matrix of partial derivatives of the components of  $\mathbf{F}$  with respect to the components of  $\mathbf{y}$ . Points  $(\mathbf{x}_0, \mathbf{y}_0)$  that satisfy the first of conditions (3.6) clearly exist because for any  $\mathbf{y}_0 \in$

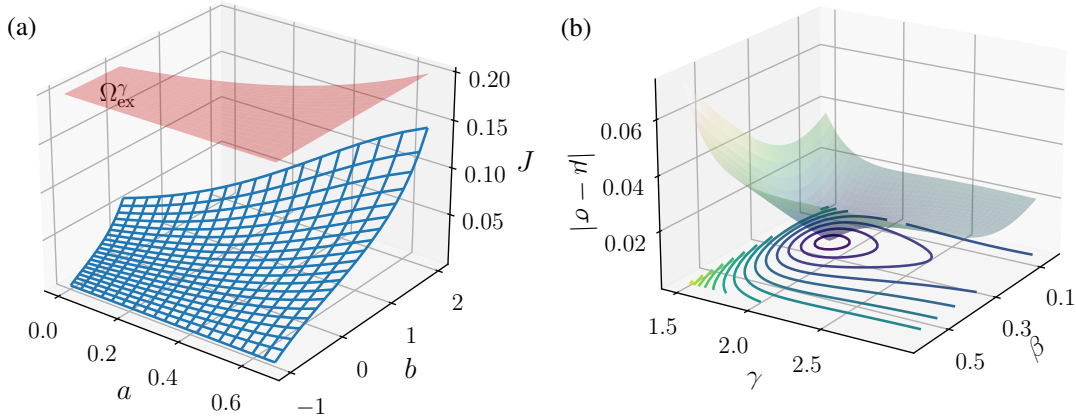


FIG. 4: (a) The Jacobian determinant  $J = \det(\partial(F_1, F_2)/\partial(a, b))$  as a function of parameters  $a$  and  $b$  for  $\beta = 0.3$  and  $\gamma = 1.5$  is shown by a blue wire frame, with the grid lines being iso-lines of the rectangular coordinates  $x$  and  $y$  defined in (2.13). The pink transparent region at the top of the axes box is the domain of excitability  $\Omega_{\text{ex}}^\gamma$ . (b) Convexity and global minimum of the distance  $|\mu - \sigma|$  between the centre of mass of the set of parameter values  $\mathcal{P}$  and that of the planar region  $\Omega_{\text{ex}}^\gamma$ , see (3.10). The values of  $\mathcal{P}$  are determined as solutions to (3.3) for the set of experimental measurements  $\mathcal{D}$  of Lachaud et al. (2022).

$\Omega_{\text{ex}}^\gamma$  a corresponding  $\mathbf{x}_0$  can be computed by evaluating the right-hand-sides of expressions (3.3), and furthermore such pairs are unique. Calculating the Jacobian determinant is straightforward but yields a lengthy expression, so to test the second of conditions (3.6) we have evaluated it numerically and plotted the surface  $J(a, b)$  over the domain  $\Omega_{\text{ex}}^\gamma$  in Figure 4(a). The plot shows that  $J$  is strictly positive even though it tends to  $0^+$  as  $b \rightarrow -1$ . The value  $b = -1$  is, of course, excluded from the open domain  $\Omega_{\text{ex}}^\gamma$  – in particular, this is the value at which the  $w$ -nullcline and the diastolic branch of the  $v$ -nullcline of the McKean model (2.1) coincide, see discussion of Figure 1(b), and it represents a non-excitable degenerate case. Thus, we conclude that a unique solution of equation (3.5) exists in  $\Omega_{\text{ex}}^\gamma$  that can be represented as

$$(a, b) = \mathbf{f}(A, \Delta A), \quad (3.8)$$

and parameters can be determined as a function of experimental data  $(A, \Delta A)$ ,

In fact, it is possible to make further progress and find a closed form solution of equation (3.3a) for the parameter  $a$  as a function of  $(b, A)$  alone, yielding

$$a = 1 - \frac{\exp(\tilde{b}\beta) \left( \exp(\tilde{b}A\beta/B) - 1 \right)}{\tilde{b} \left( \exp(\tilde{b}\beta) - 1 \right) \exp(\tilde{b}A\beta/B)}, \quad \tilde{b} = 1 + b. \quad (3.9)$$

However, equation (3.3b) is rather more difficult to solve explicitly for  $b$ . For this reason, we resort to solving equations (3.3) numerically for both  $a$  and  $b$ . Numerical solution is straightforward: for completeness, we mention that we have used the modified Powell hybrid method (Powell, 1970) as implemented in the SciPy numerical library (Virtanen et al., 2020).

### 3.3 Calibration of BCL and drug dose

Equations (3.3) contain, in fact,  $2N + 2$  unknown parameters – in addition to  $a_i$  and  $b_i$ , the BCL  $\beta$  and the drug dose parameter  $\gamma$  to be used with the model equations are also not known a priori. To proceed with the analysis, unique values of  $\beta$  and  $\gamma$  must be selected employing a plausible assumption. In the absence of additional criteria, we impose the requirements (a) that all solutions  $(a_i, b_i)$ ,  $i = 1, \dots, N$  belong to the domain of excitability  $\Omega_{\text{ex}}^\gamma$  and (b) that these solutions are distributed so that the distance between their centre of mass and the centre of mass of the planar region  $\Omega_{\text{ex}}^\gamma$  is minimal. We will refer to this as the “optimal excitability” assumption as it requires that points are located as far away as possible from the boundaries of the excitability domain, outside of which the system is, of course, non-excitable. Indeed, there is no prior expectation or experimental evidence that the distribution is biased in any direction. Thus, we determine the values of  $\beta$  and  $\gamma$  as

$$(\beta^*, \gamma^*) = \arg \min_{(\beta, \gamma)} \left| \mu(\beta, \gamma) - \sigma(\beta, \gamma) \right| \quad \text{s.t.} \quad (a_i(\beta^*, \gamma^*), b_i(\beta^*, \gamma^*)) \in \Omega_{\text{ex}}^\gamma \quad \forall i = 1, \dots, N, \quad (3.10a)$$

where  $\mu$  is the position vector of the centre of mass of the set  $\mathcal{P}(\beta, \gamma)$  of discrete points  $(a_i, b_i)$ ,  $i = 1, \dots, N$  with coordinates in the  $(a, b)$ -plane computed as the arithmetic means

$$\mu[\mathcal{P}(\beta, \gamma)] := \frac{1}{N} \left( \sum_{i=1}^N a_i(\beta, \gamma), \sum_{i=1}^N b_i(\beta, \gamma) \right), \quad (3.10b)$$

and  $\sigma$  is the position vector of the centre of mass of the planar region  $\Omega_{\text{ex}}^\gamma$  which has coordinates in the  $(a, b)$  plane given by

$$\sigma[\Omega_{\text{ex}}^\gamma(\beta, \gamma)] = \left( \log \frac{\gamma}{\gamma-1} - \frac{1}{\gamma}, \log \frac{\gamma-1}{\gamma} + \frac{1}{2(\gamma-1)} \right) \Big/ \log \frac{\gamma}{\gamma-1}. \quad (3.10c)$$

Criterion (3.10) constitutes a nonlinear minimisation problem with constraints and it is not easy to establish whether a unique solution to it exists. Here once again, we will restrict the effort to a numerical demonstration instead. In Figure 4(b) contour lines of the objective minimisation surface, the distance  $|\mu - \sigma|$ , are plotted in the  $(\beta, \gamma)$  plane for the distribution of parameter values  $(a_i, b_i)$  determined from the experimental measurements  $(A_i, \Delta A_i)$  of Lachaud et al. (2022). The plot shows that the surface is globally convex and has a single minimum, indeed. While short of a rigorous proof, this provides an indication that a single global minimum exists that will allow to find unique values for the model BCL  $\beta$  and the model drug dose parameter  $\gamma$ .

To ensure robustness, we employ a stochastic method for constrained global optimisation of multi-modal multi-variate objective functions to solve the minimisation problem (3.10). The method is a combination of classical and fast simulated-annealing approaches (Tsallis & Stariolo, 1996), coupled to a strategy for applying a local search at accepted locations (Xiang & Gong, 2000). We use the SciPy numerical library implementation of this dual annealing optimisation (Virtanen et al., 2020) which has been benchmarked in (Mullen, 2014). Results of this approach are presented in the next subsection.

### 3.4 Results

Figure 5(a) shows the experimentally measured data set  $\mathcal{D}(\mathcal{B}, \Gamma) = \{(A_i, \Delta A_i), i = 1, \dots, N\}$ , the values of which are obtained from (Lachaud et al., 2022). Figure 5(b) shows the corresponding set of

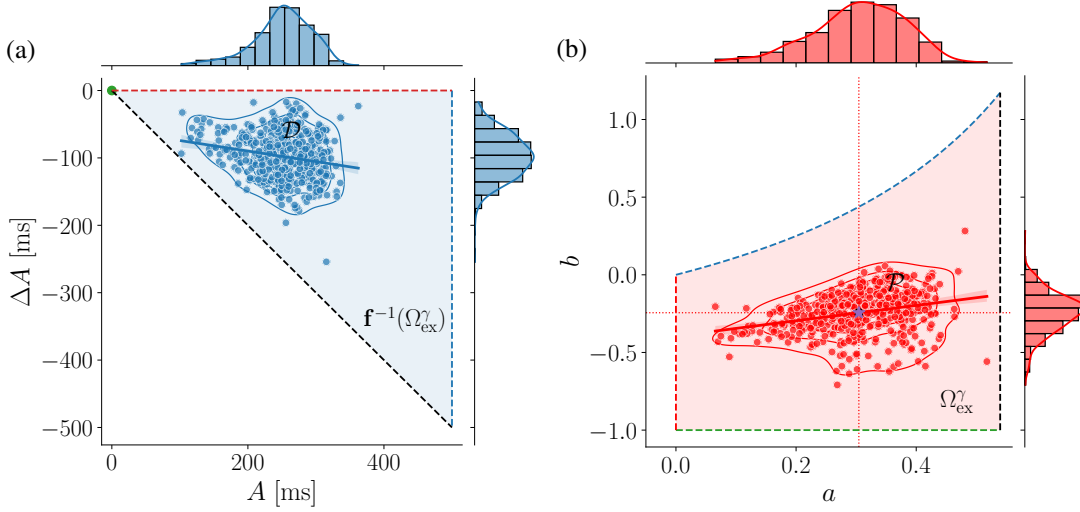


FIG. 5: (a) Scatter plot of the set  $\mathcal{D}(B, \Gamma)$  of 496 experimental measurements at  $B = 500$  ms and  $\Gamma = 1$   $\mu\text{M}$  nifedipine, data due to (Lachaud et al., 2022) c.f. their figure 3C(iii). (b) Scatter plot of the set  $\mathcal{P}(\beta^*, \gamma^*)$  of corresponding McKean parameters obtained by numerical solution of the inverse problem (3.3) with calibrated  $\beta^* = 0.23487$  and  $\gamma^* = 1.85262$ . Thin dotted lines denote the locations of the mean values of  $a_i$  and  $b_i$  with their intersection being the centre of mass  $\mu$  of  $\mathcal{P}$  and the violet star marker is the centre of mass  $\sigma$  of  $\Omega_{\text{ex}}^\gamma$ . The shaded areas are the parameter region for excitable dynamics  $\Omega_{\text{ex}}^\gamma$  in (b) and its pre-image in (a). Histogram distributions with Gaussian kernel density estimations and simple data regression lines are also plotted in both panels.

solutions  $\mathcal{P} = \{(a_i, b_i), i = 1, \dots, N\}$  of the problem given by equations (3.3) and (3.10). It has been obtained numerically and is a graphical representation of the main outcome of the approach described above. Practically, the solution procedure involves for each pair of  $\beta$  and  $\gamma$  constructing the domain of excitability  $\Omega_{\text{ex}}^\gamma$  from equation (3.4), numerically solving the inverse problem (3.3) on this domain, computing the distance between the respective centres of mass from equation (3.10b,c), and minimising this distance with respect to  $\beta$  and  $\gamma$  as per (3.10a). For the given experimental dataset, this calibration procedure fixes the values of the basic cycle length and the drug dose parameter of the model to

$$\beta^* = 0.23487, \quad \gamma^* = 1.85262, \quad (3.11)$$

which results in the centres of mass of  $\mathcal{P}$  and  $\Omega_{\text{ex}}^\gamma$  located at a distance  $|\mu - \sigma| < 1.2 \times 10^{-9}$  apart at

$$(a^*, b^*) = (0.30450246, -0.24420404). \quad (3.12)$$

The domain of excitability  $\Omega_{\text{ex}}^\gamma$  in the  $(a, b)$  plane and its pre-image  $\mathbf{f}^{-1}(\Omega_{\text{ex}}^\gamma)$  in the  $(A, \Delta A)$  plane, see equation (3.8), are shown in Figure 5(a) and (b), respectively. The size and shape of  $\Omega_{\text{ex}}^\gamma$  depend on the drug dose parameter  $\gamma$ . The boundaries of the image and pre-image are coloured correspondingly in panels (a) and (b) of Figure 5 to illustrate how they map into each other. It is interesting to note that the curve  $b = -1$  maps into a single point  $(0, 0)$  in the  $(A, \Delta A)$  plane and from the plot of the values of the Jacobian determinant in Figure 4(a) numerical solution of the inverse problem is expected to be

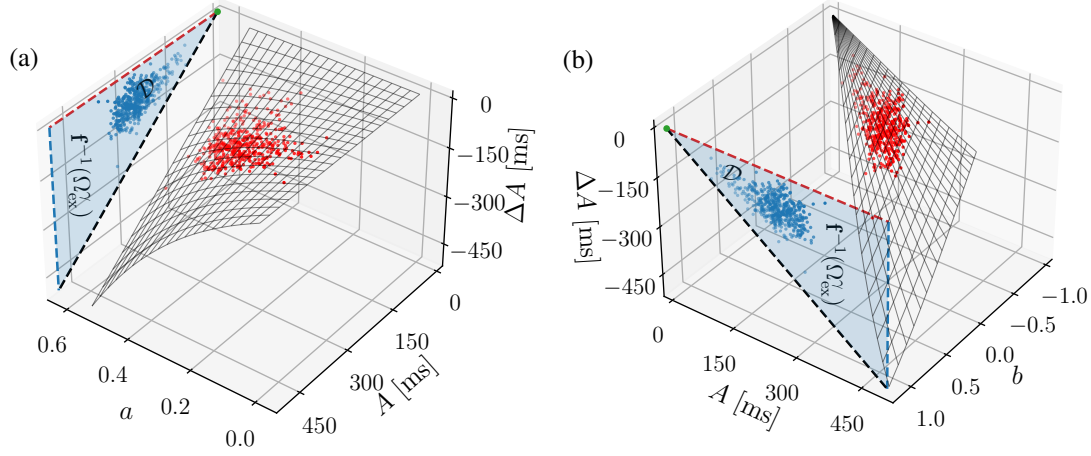


FIG. 6: McKean model parameters  $a$  and  $b$  as functions of  $A$  and  $\Delta A$  shown as wireframe surfaces in panel (a) and (b), respectively. Scatter plot of the experimental data  $\mathcal{D}$  of Lachaud et al. (2022) is shown as blue dots and its projections onto the surfaces  $a(A, \Delta A)$  and  $b(A, \Delta A)$  are shown as red dots.

most challenging in the vicinity of this point. The relation  $\mathbf{f}^{-1}$ , which may be seen as a change of variables transformation, maps the curves  $a = 0$ ,  $b = a/(1 - a)$  and  $a = 1/\gamma$  into the straight lines  $\Delta A = 0$ ,  $A = B$ , and  $\Delta A = -A$ , respectively. Thus, the pre-image  $\mathbf{f}^{-1}(\Omega_{\text{ex}}^\gamma)$  does not depend on  $\beta$  and  $\gamma$  and has a triangular shape in the  $(A, \Delta A)$  plane. This agrees with the analysis of Lachaud et al. (2022) where this region was empirically determined, see their figure 3C(iii). It is also remarkable to observe how well the set of experimental measurements  $\mathcal{D}(B, \Gamma)$  is distributed and oriented within  $\mathbf{f}^{-1}(\Omega_{\text{ex}}^\gamma)$ .

Histograms, gaussian kernel density estimations and simple data regression lines of the sets  $\mathcal{D}$  and  $\mathcal{P}$  are also plotted in Figure 5. Such measures are routinely used in the analysis of experimental results, and can be compared e.g. to figure 3C(iii) of (Lachaud et al., 2022). Further descriptive statistical analysis of these results can be performed but remains beyond the focus of the paper.

The map  $\mathbf{f}$  introduced as a calibrated solution of equations (3.3) and its inverse  $\mathbf{f}^{-1}$  are both vector-valued functions of two arguments

$$\mathbb{R}^2 \ni (A, \Delta A) \begin{matrix} \xrightarrow{\mathbf{f}} \\ \xleftarrow{\mathbf{f}^{-1}} \end{matrix} (a, b) \in \mathbb{R}^2.$$

Therefore, Figure 5 is insufficient to identify graphically how experimental data points in the  $(A, \Delta A)$  plane map to parameter value points in the  $(a, b)$  plane. To visualise this relationship more directly, we have plotted in Figure 6 the two components of  $\mathbf{f} = (f_1, f_2)$ , namely  $a = f_1(A, \Delta A)$  and  $b = f_2(A, \Delta A)$ , separately. This allows to map the physiological measures into model parameters, in particular, to identify the value of  $a_i$  that corresponds to a given data point  $(A_i, \Delta A_i)$  from panel (a) and the value of  $b_i$  that corresponds to the same data point  $(A_i, \Delta A_i)$  from panel (b). The surfaces  $a(A, \Delta A)$  and  $b(A, \Delta A)$  are shown as wire-frames with grid lines that are iso-lines of the rectangular coordinates  $x$  and  $y$  defined by equation (2.13) in earlier sections. This figure highlights the fact that an experimentally measured value of the action potential duration  $A$  is not sufficient to characterise the cellular properties of a myocyte.

Indeed, a fixed value of  $A$  corresponds to entire intervals as opposed to unique values for the parameters  $a$  and  $b$  as evident in panels (a) and (b), respectively. This point is further discussed in the next section.

## 4. Discussion and predictions

### 4.1 Parameter interrelationships

The main conclusions made in the work of [Lachaud et al. \(2022\)](#) are (a) “that AP morphology is retained by relationships linking specific ionic conductances” and (b) that “these interrelationships are necessary for stable repolarization despite large inter-cell variation of individual conductances and this explains the variable sensitivity to ion channel block”. In an attempt to verify this assertion and to determine such interrelationships explicitly, we have plotted a family of curves

$$\begin{aligned} \mathcal{C}_a &= (A, \Delta A)|_{(a=\text{const}, b)}, & \mathcal{C}_b &= (A, \Delta A)|_{(a, b=\text{const})}, \\ \mathcal{C}_A &= (a, b)|_{(A=\text{const}, \Delta A)}, & \mathcal{C}_{\Delta A} &= (a, b)|_{(A, \Delta A=\text{const})}; \end{aligned}$$

the first pair in Figure 7(a) and the second pair in in Figure 7(b), respectively. For example, a curve of the type  $\mathcal{C}_A$  represents the interrelationship which the internal model parameters must satisfy so that the value of APD remains constant, and similarly for the other types. We observe that the situation is more involved than suggested by [Lachaud et al. \(2022\)](#) in that interrelationship represented by  $\mathcal{C}_A$  changes with the particular APD value, as well. For instance, for  $A = 0$  ms and small values of  $A$  the dependence on  $a$  is insignificant, or there is an approximately linear relationship between  $a$  and  $b$ , while for larger values of  $A$  the relationship approaches  $b = 1/(1-a)$ , which is the respective boundary of the excitability domain  $\Omega_{\text{ex}}^\gamma$ . Similar remarks hold for the other “grid” lines in Figure 7. We wish to note that some of the interrelationships have already been obtained in closed in the preceding sections. Indeed, the “grid” lines  $\mathcal{C}_a$  and  $\mathcal{C}_b$  plotted in Figure 7(a) are given by the general expression (2.12a). Similarly, curves  $\mathcal{C}_A$  and  $\mathcal{C}_{\Delta A}$  are given by equation (3.9) derived in section 3.2 in relation to the conditions for solution of problem (3.3) when evaluated for specified values of  $A$  and  $\Delta A$ .

### 4.2 Dependence on drug concentration and basic cycle length

The McKean model does not offer a close correspondence to electrophysiological myocyte structures, as conceded already, including in the title of the article. However, the strength of our approach is that, in addition to theoretical insight, it is possible and rather economical to make simple predictions that can be tested by (or indeed guide) experimental measurements. Figures 8(a) and (b) show predictions of how the experimental myocyte scatter cloud  $\mathcal{D}$  morphs when drug concentration  $\Gamma$  and basic cycle length  $B$  are varied, respectively. To produce these predictions, it is assumed that a preliminary reference experiment at fixed values of BCL and drug concentration, say  $B^*$  and  $\Gamma^*$ , has been performed. The set  $\mathcal{P}$  of corresponding McKean model parameter values is then estimated by solving (3.3) and (3.10) with reference values  $\beta^*$  and  $\gamma^*$  determined simultaneously as discussed in section 3. Here, for example, we continue to use the data of [Lachaud et al. \(2022\)](#) which has  $B^* = 500$  ms and  $\Gamma^* = 1 \mu\text{M}$  nifedipine and calibration yields  $\beta^* = 0.23487$  and  $\gamma^* = 1.85262$  as before. The calculated cell-specific values  $(a_i, b_i)$ ,  $i = 1, \dots, N$ , are then used as arguments in the asymptotic expression for APD and  $\Delta\text{APD}$ , in fact expressions (3.3) once again but with now varying the values of  $\beta$  and  $\gamma$  away from  $\beta^*$  and  $\gamma^*$ . Finally, results are converted to dimensional units using the scaling transformations

$$\Gamma = \Gamma^* \frac{\gamma - 1}{\gamma^* - 1}, \quad B = B^* \frac{\beta}{\beta^*}. \quad (4.1)$$



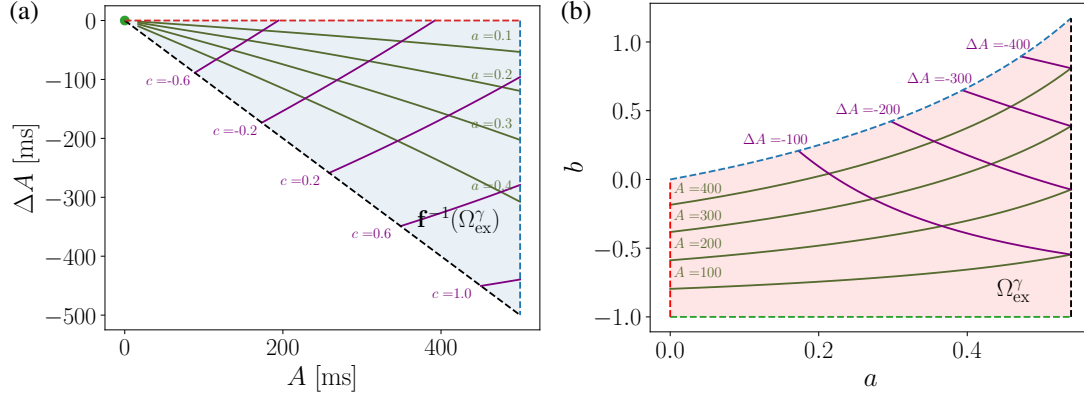


FIG. 7: (a) Lines in the  $(A, \Delta A)$  plane obtained at constant values of  $a$  (olive green) and at constant values of  $b$  (purple) as labeled in the vicinity of each curve. (b) Lines in the  $(a, b)$  plane obtained at constant values of  $A$  (olive green) and at constant values of  $\Delta A$  (purple) as indicated in the vicinity of each curve. In both panels  $\beta = 0.23487$  and  $\gamma = 1.85262$ . Other elements of the plot are similar to these described in the caption of Figure 5.

With decrease of the drug dose the change in action potential duration decreases as expected. With increase of drug dose  $\Gamma$  the myocyte cloud extends down to increasingly more negative values of  $\Delta A$  i.e. the drug increasingly shortens APD. The pre-image of the excitability domain does not depend on  $\Gamma$ , as discussed further above, and points of the myocyte cloud eventually drift outside of it. Indeed, increasing the drug dose makes a proportion of the cell population non-excitable. This proportion can be estimated with respect to the reference experiment as

$$L = 1 - \frac{\int_{\Omega_{\text{ex}}^\gamma} dS}{\int_{\Omega_{\text{ex}}^{\gamma^*}} dS} = 1 - \frac{\log((\gamma - 1)/\gamma)}{\log((\gamma^* - 1)/\gamma^*)}, \quad (4.2)$$

where, for simplicity, we have assumed that cell properties are uniformly distributed within their excitability domains and the ‘‘coefficient of loss’’  $L$  is the ratio of the planar area of  $\Omega_{\text{ex}}^\gamma$  at concentration  $\gamma$  and planar area of  $\Omega_{\text{ex}}^{\gamma^*}$  at the reference concentration  $\gamma^*$ . Equation (4.2) can be re-cast in terms of drug concentration  $\Gamma$  with the help of the change of variables (4.1). With variation of the basic cycle length  $B$  the myocyte cloud seems to undergo a shape-preserving scaling transformation - it enlarges with increase of  $B$  or shrinks with decrease of  $B$  while keeping shape as seen in Figure 8(b). The pre-image  $\mathbf{f}^{-1}(\Omega_{\text{ex}}^\gamma)$  does change size in a similar way with  $B$ . The myocyte cloud scales non-linearly as determined by equation (2.12a) and illustrated in the restitution curve of Figure 3(b) and would thus ‘‘saturate’’ for values of  $B$  larger than shown in Figure 8(b).

#### 4.3 Dose-response curves

Perhaps most significant from a control and medical intervention viewpoint is the problem to determine a ‘‘target’’ value of the drug concentration,  $\Gamma_T$  say, to be administered to a population of myocytes such that all myocytes respond with an identical target ‘‘healthy’’ action potential under periodic stimulation. We will denote the duration of this target AP by  $A_T$ . The target concentration  $\Gamma_T$  sought will be different

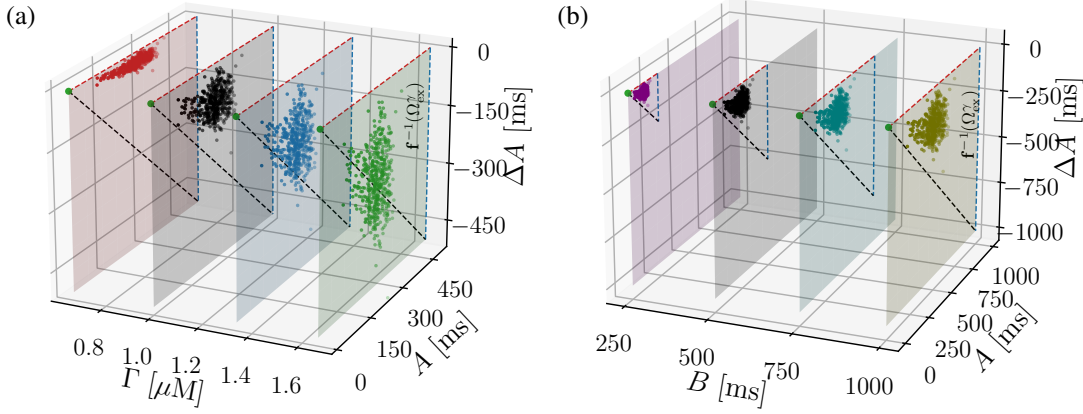


FIG. 8: Prediction for the spread of the experimental data-point distribution  $\mathcal{D}$  of Lachaud et al. (2022) (black cloud) with variation of the drug concentration  $\Gamma$  in (a) the basic cycle length  $B$  in (b).

for each cell in the population. Assuming as before that a preliminary reference experiment has been performed at fixed  $B^*$  and  $\Gamma^*$ , that  $\beta^*$  and  $\gamma^*$  have been calibrated and the McKean parameters have been determined then the target drug concentration  $\Gamma_T$  is given by

$$\Gamma_T = \frac{\Gamma^*}{\gamma^* - 1} \left( \frac{1}{a} - \frac{\exp(\tilde{b}\beta^*) \left( \exp(\tilde{b}A_T\beta^*/B^*) - 1 \right)}{a\tilde{b} \left( \exp(\tilde{b}\beta^*) - 1 \right) \exp(\tilde{b}A_T\beta^*/B^*)} - 1 \right), \quad \tilde{b} = 1 + b. \quad (4.3)$$

The latter is, of course, precisely expression (3.9) where the target value of the McKean “conductance” parameter is related to the one determined in the reference experiment by  $a_T = \gamma_T a$  and scaling (4.1) to dimensional values has been applied. Further, values of  $\gamma_T$  determined from this expression must be additionally subjected to the (a) constraints  $\gamma_T > 1$  or equivalently  $\Gamma_T > 0 \mu\text{M}$  nif and (b)  $\gamma_T < 1/a$ . Constraint (a) reflects the fact that the minimal drug concentration that can be administered is  $0 \mu\text{M}$ , and constraint (b) is the, now familiar, requirement that for a cell to be excitable  $a\gamma_T < 1$  must hold. Figure 9(a) illustrates these results and shows the target drug concentration values for nifedipine in  $\mu\text{M}$  with values  $\beta^*$  and  $\gamma^*$  calibrated for the data of Lachaud et al. (2022). The surface  $\Gamma_T$ , logarithmically transformed for clarity of visualisation, is plotted both as a function of the experimental biomarkers of the controlled experiment ( $A, \Delta A$ ) and a similar plot can be constructed in terms of corresponding McKean model parameters ( $a, b$ ). While constraint (b) appears to be always satisfied, constraint (a) restricts the range of myocytes for which the drug intervention can work. This is easy to understand – as nifedipine is an APD shortening drug, for cells with APD already shorter than the target APD, there is no amount of nifedipine that can be administered to prolong APD to the target value. A second drug with a different mechanism may, of course, be deployed.

It is, of course, not possible to administer different drug dose to each individual cell. Figure 9(b) provides more conventional dose-response curves computed using equation (3.3b) for each cell in the population as well as a for the “mean cell” in the population, the point with parameter values given

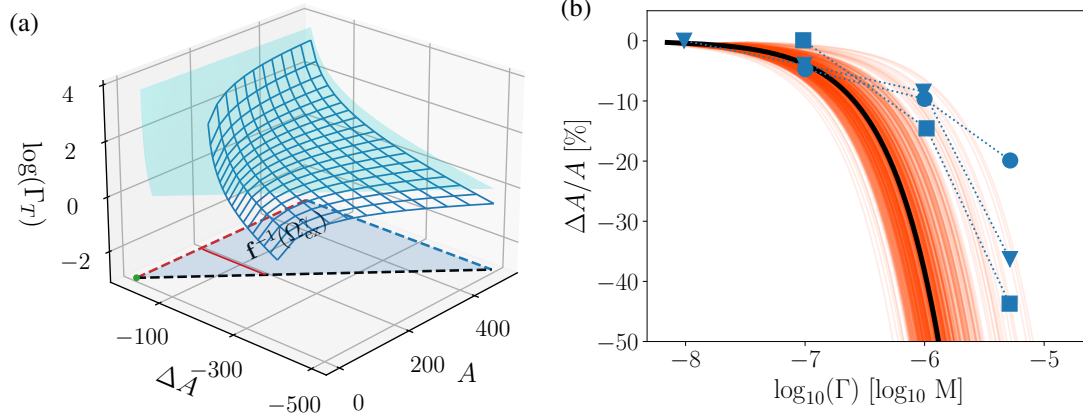


FIG. 9: (a) Values  $\Gamma_T$  of the drug concentration (nifedipine in  $\mu\text{M}$ ) necessary to elicit action potentials with a prescribed duration  $A_T = 180$  ms in a heterogeneous population of myocytes (blue wireframe surface). The solid red line is a projection of the line  $\Gamma_T = 0$   $\mu\text{M}$  and the transparent aquamarine surface is  $\Gamma_T = \Gamma^* (1 - a) / (\gamma^* - 1) / a$ , both constraining the acceptable values  $\Gamma_T$  can take. (b) Dose-response curve of nifedipine computed using (3.3b). Thin semi-transparent lines are dose-response curves for individual cells in the myocyte population of Lachaud et al. (2022), with the solid black line corresponding to the “mean cell” with parameter values given in (3.12). Experimental data (blue dotted lines) from rabbit Purkinje fibre action potentials (triangles down) and ventricular action potentials (circles) and field potentials (squares) in thin-slice tissue preparations is also shown (data from figure 6B of (Himmel et al., 2012)). In both panels, McKean parameters ( $a, b$ ) are calibrated to experimental data of Lachaud et al. (2022) using  $B^* = 500$  ms,  $\Gamma^* = 1$   $\mu\text{M}$  nif. and  $\beta^* = 0.23487$  and  $\gamma^* = 1.85262$ .

in equation (3.12). These predicted dose-response curves are also compared in the Figure to experimental data from (Himmel et al., 2012) where the dose response to nifedipine was measured by the changes elicited in action potentials and field potentials in thin slices of rabbit ventricular tissue and rabbit Purkinje fibres. The results show a remarkable agreement, given there are very significant differences in experimental configuration (tissue slices as opposed uncoupled cells), types of measurement (field potentials in some cases) and the essential variation in cellular properties (Purkinje as opposed to ventricular myocytes, also unrelated animals) that is now known to exist between populations. The latter heterogeneity has been the underlying motivation for the present work.

## 5. Conclusion

In this work, a simple conceptual model of cellular excitability is employed to analyse experimental measurements of ion channel block in a large and heterogeneous population of uncoupled cardiomyocytes. The experimental data, due to Lachaud et al. (2022), consists principally of values of the action potential duration shortening measured in nearly 500 rabbit ventricular myocytes to which 1  $\mu\text{M}$  of the drug nifedipine was applied. The cells were sourced from various regions of the left ventricles of several different animals and exhibited a significant intrinsic variation in their action potential duration

and drug response, already quantified by [Lachaud et al. \(2022\)](#). The main aim of our analysis is to infer the cellular properties of each myocyte in terms of cell-specific parameter values of an appropriate mathematical model and the [McKean \(1970\)](#) model was selected for this purpose due to its simplicity. The [McKean \(1970\)](#) model is a fast-slow system of piece-wise linear ordinary differential equations of FitzHugh-Nagumo type. It has two variables that can be interpreted as voltage and an effective gating variable and two intrinsic parameters that can be seen as an effective ion current conductance and an effective kinetic parameter. Here, the domain in parameter space where the model exhibits excitable dynamics (as opposed to oscillatory or bistable) is determined, and an asymptotic approximation of the duration of 1:1 action potentials generated by strictly periodic stimulation is obtained using a standard fast-slow asymptotic analysis ([Tikhonov, 1952](#); [Fenichel, 1979](#)). The approximation takes the form of an explicit analytical expression for the APD as a function of the [McKean \(1970\)](#) model parameters and the basic cycle length of stimulation, i.e.  $\alpha(a, b, \beta)$ . Such a relation is known as a restitution curve/relation in the electrophysiological literature. The drug action of nifedipine is modelled by introducing a multiplicative factor  $\gamma$  to the effective conductance parameter  $a$ , yielding a problem for the solution of a set of non-linear algebraic equations from which the McKean model parameters  $a_i$  and  $b_i$  for each cell  $i = 1, \dots, N$ , can be determined given experimental measurements of the action potential durations  $A_i$  and  $A_i + \Delta A_i$  recorded under periodic stimulation with basic cycle length  $B$  before and after drug application with concentration  $\Gamma$ . Remarkably, this results in an adaptive domain problem, where the parameter domain  $\Omega_{\text{ex}}^\gamma(\beta, \gamma)$ , the basic cycle length  $\beta$  and the drug dose parameter  $\gamma$  must be determined as a part of the solution. This is done by introducing a further modelling assumption that the euclidean distance between its centroid of the domain and the algebraic mean of the McKean parameter values of the population is minimal. It is demonstrated by direct numerical evaluation that (a) the adaptive domain minimisation and (b) the set of  $2N$  nonlinear algebraic equations both admit unique solutions, that are then found using standard numerical routines. In particular, the existence of  $\Omega_{\text{ex}}^\gamma(\beta, \gamma)$  different from  $\Omega_{\text{ex}}(\beta, \gamma)$ , suggests that (when implementing heterogeneity in realistic models, parameter values should be selected from a restricted region of the parameter space only. The results are then also used (a) to understand interrelationships proposed by [Lachaud et al. \(2022\)](#) as necessary to ensure generation of stable AP morphology and repolarisation, (b) to predict the scatter of APD values of the population with variation of basic cycle length and drug concentration, (c) to calculate nifedipine drug-response curves for each cell in the population and determine a value for the drug concentration required so that each uncoupled cell, and the population as a whole, responds with a single APD value, and (d) predict the proportion of cells that become inexcitable at large drug doses. Prediction (c) is found to compare well with independent experimental measurements ([Himmel et al., 2012](#)), while the other predictions may also be tested or indeed guide experimental measurements.

The methodology presented here can be extended, refined and applied in a number of directions. (a) Being piece-wise linear, the [McKean \(1970\)](#) model allows exact solutions in closed form and thus the asymptotic expression (2.12a) used here may be replaced by more a more accurate exact expression. This will then allow to incorporate experimental measurements of secondary AP biomarkers, such as action potential duration at 50% and 30% from peak, impossible to distinguish using the present asymptotic expression. (b) In place of the [McKean \(1970\)](#) model, the caricature Noble model proposed by [Biktashev et al. \(2008a\)](#) as an archetypal model of cardiac excitability may be used. It has the advantage of having been derived by a controlled and systematic procedure from an actual ionic current model and captures the fundamental mathematical structure of cardiac electrical excitability. In particular, it includes a super-fast subsystem, lacking in the [McKean \(1970\)](#) model, which will allow analysis of biomarkers describing the front (Phase 1) of the action potential, such as the time from 10% to 90% of upstroke (TRise) which has been also measured experimentally and depends on cellular processes

essentially different from these that control action potential duration. The caricature Noble model has been recently fitted to reproduce the action potential morphology and restitution properties of several cardiomyocyte phenotypes (Aziz & Simatev, 2022) and has known exact and asymptotic solutions (Biktashev et al., 2008a; Simatev & Biktashev, 2011), albeit more involved. (c) In our work only the drug action on the effective conductance parameter  $a$  is considered, and the attention is further restricted to the case of action potential shortening as needed for comparison to the nifedipine dataset of Lachaud et al. (2022). The cases of action potential prolongation and of drug action applied to the effective kinetic parameter  $b$  need to be investigated, as well. Action potential prolongation is induced for instance by the drug dofetilide with measurements also reported in (Lachaud et al., 2022). In this case the parameter domain of excitability must be adapted in a different way meriting a separate investigation. (d) It will be of interest to extend the current methodology to include coupling between myocytes and thus investigate AP waveform synchronisation. This is likely to play a significant role in generation a stable action potential response on tissue-wide level. These are all directions open for future research.

**ACKNOWLEDGEMENTS** This work was supported by the UK Engineering and Physical Sciences Research Council [grant numbers EP/S030875/1 and EP/T017899/1].

## References

- Aliev, R. R. & Panfilov, A. V. (1996). A simple two-variable model of cardiac excitation. *Chaos, Solitons & Fractals*, 7(3), 293–301, doi:[10.1016/0960-0779\(95\)00089-5](https://doi.org/10.1016/0960-0779(95)00089-5). 3
- Anumonwo, J. M. & Pandit, S. V. (2015). Ionic mechanisms of arrhythmogenesis. *Trends in Cardiovascular Medicine*, 25(6), 487–496, doi:[10.1016/j.tcm.2015.01.005](https://doi.org/10.1016/j.tcm.2015.01.005). 1
- Aziz, M. H. N. & Simatev, R. D. (2022). Estimation of Parameters for an Archetypal Model of Cardiomyocyte Membrane Potentials. To appear in *International Journal of Bioautomation*. 21
- Barkley, D. (1991). A model for fast computer simulation of waves in excitable media. *Physica D: Nonlinear Phenomena*, 49(1-2), 61–70, doi:[10.1016/0167-2789\(91\)90194-e](https://doi.org/10.1016/0167-2789(91)90194-e). 8
- Bassingthwaighe, J. B. (2000). Strategies for the Physiome Project. *Annals of Biomedical Engineering*, 28(8), 1043–1058, doi:[10.1114/1.1313771](https://doi.org/10.1114/1.1313771). 2
- Bers, D. M. (2001). *Excitation-Contraction Coupling and Cardiac Contractile Force*. Springer Netherlands. 1
- Bezekci, B., Idris, I., Simatev, R. D., & Biktashev, V. N. (2015). Semianalytical approach to criteria for ignition of excitation waves. *Physical Review E*, 92(4), doi:[10.1103/physreve.92.042917](https://doi.org/10.1103/physreve.92.042917). 4
- Biktashev, V. N., Suckley, R., Elkin, Y. E., & Simatev, R. D. (2008a). Asymptotic Analysis and Analytical Solutions of a Model of Cardiac Excitation. *Bulletin of Mathematical Biology*, 70(2), 517–554, doi:[10.1007/s11538-007-9267-0](https://doi.org/10.1007/s11538-007-9267-0). 3, 20, 21
- Biktashev, V. N., Suckley, R., Elkin, Y. E., & Simatev, R. D. (2008b). Asymptotic Analysis and Analytical Solutions of a Model of Cardiac Excitation. *Bulletin of Mathematical Biology*, 70(2), 517–554, doi:[10.1007/s11538-007-9267-0](https://doi.org/10.1007/s11538-007-9267-0). 9
- Brennan, T., Fink, M., & Rodriguez, B. (2009). Multiscale modelling of drug-induced effects on cardiac electrophysiological activity. *European Journal of Pharmaceutical Sciences*, 36(1), 62–77, doi:[10.1016/j.ejps.2008.09.013](https://doi.org/10.1016/j.ejps.2008.09.013). 11
- Clayton, R., et al. (2011). Models of cardiac tissue electrophysiology: Progress, chal-

- lenges and open questions. *Progress in Biophysics and Molecular Biology*, 104(1-3), 22–48, doi:[10.1016/j.pbiomolbio.2010.05.008](https://doi.org/10.1016/j.pbiomolbio.2010.05.008). 2
- Clayton, R. H., et al. (2020). An audit of uncertainty in multi-scale cardiac electrophysiology models. *Philosophical Transactions of the Royal Society A: Mathematical, Physical and Engineering Sciences*, 378(2173), 20190335, doi:[10.1098/rsta.2019.0335](https://doi.org/10.1098/rsta.2019.0335). 2, 3
- Clerx, M., Beattie, K. A., Gavaghan, D. J., & Mirams, G. R. (2019). Four Ways to Fit an Ion Channel Model. *Biophysical Journal*, 117(12), 2420–2437, doi:[10.1016/j.bpj.2019.08.001](https://doi.org/10.1016/j.bpj.2019.08.001). 3
- Cooper, J., Scharm, M., & Mirams, G. R. (2016). The Cardiac Electrophysiology Web Lab. *Biophysical Journal*, 110(2), 292–300, doi:[10.1016/j.bpj.2015.12.012](https://doi.org/10.1016/j.bpj.2015.12.012). 3
- Corrias, A., Jie, X., Romero, L., Bishop, M. J., Bernabeu, M., Pueyo, E., & Rodriguez, B. (2010). Arrhythmic risk biomarkers for the assessment of drug cardiotoxicity: from experiments to computer simulations. *Philosophical Transactions of the Royal Society A: Mathematical, Physical and Engineering Sciences*, 368(1921), 3001–3025, doi:[10.1098/rsta.2010.0083](https://doi.org/10.1098/rsta.2010.0083). 1
- Coveney, S. & Clayton, R. H. (2020). Sensitivity and Uncertainty Analysis of Two Human Atrial Cardiac Cell Models Using Gaussian Process Emulators. *Frontiers in Physiology*, 11, doi:[10.3389/fphys.2020.00364](https://doi.org/10.3389/fphys.2020.00364). 3
- Coveney, S., Corrado, C., Oakley, J. E., Wilkinson, R. D., Niederer, S. A., & Clayton, R. H. (2021). Bayesian Calibration of Electrophysiology Models Using Restitution Curve Emulators. *Frontiers in Physiology*, 12, doi:[10.3389/fphys.2021.693015](https://doi.org/10.3389/fphys.2021.693015). 3
- Crumb, W. J., Vicente, J., Johannesen, L., & Strauss, D. G. (2016). An evaluation of 30 clinical drugs against the comprehensive in vitro proarrhythmia assay (CiPA) proposed ion channel panel. *Journal of Pharmacological and Toxicological Methods*, 81, 251–262, doi:[10.1016/j.vascn.2016.03.009](https://doi.org/10.1016/j.vascn.2016.03.009). 10
- Darbar, D. (2018). Standard Antiarrhythmic Drugs. In *Cardiac Electrophysiology: From Cell to Bedside* (pp. 1062–1075). Elsevier. 1
- Davies, M. R., et al. (2016). Recent developments in using mechanistic cardiac modelling for drug safety evaluation. *Drug Discovery Today*, 21(6), 924–938, doi:[10.1016/j.drudis.2016.02.003](https://doi.org/10.1016/j.drudis.2016.02.003). 2
- Fall, C. P., Marland, E. S., Wagner, J. M., & Tyson, J. J., Eds. (2004). *Computational Cell Biology*. Springer New York. 8
- Feeny, A. K., et al. (2020). Artificial Intelligence and Machine Learning in Arrhythmias and Cardiac Electrophysiology. *Circulation: Arrhythmia and Electrophysiology*, 13(8), doi:[10.1161/circep.119.007952](https://doi.org/10.1161/circep.119.007952). 3
- Fenichel, N. (1979). Geometric singular perturbation theory for ordinary differential equations. *Journal of Differential Equations*, 31(1), 53 – 98, doi:[10.1016/0022-0396\(79\)90152-9](https://doi.org/10.1016/0022-0396(79)90152-9). 6, 20
- FitzHugh, R. (1961). Impulses and Physiological States in Theoretical Models of Nerve Membrane. *Biophysical Journal*, 1(6), 445–466, doi:[10.1016/s0006-3495\(61\)86902-6](https://doi.org/10.1016/s0006-3495(61)86902-6). 3, 4
- Gemmell, P., Burrage, K., Rodríguez, B., & Quinn, T. A. (2016). Rabbit-specific computational modelling of ventricular cell electrophysiology: Using populations of models to explore variability in the response to ischemia. *Progress in Biophysics and Molecular Biology*, 121(2), 169–184, doi:[10.1016/j.pbiomolbio.2016.06.003](https://doi.org/10.1016/j.pbiomolbio.2016.06.003). 2, 3
- Hastie, T., Tibshirani, R., & Friedman, J. (2009). *The Elements of Statistical Learning*. Springer New York. 3
- Himmel, H. M., Bussek, A., Hoffmann, M., Beckmann, R., Lohmann, H., Schmidt, M., & Wettwer,

- E. (2012). Field and action potential recordings in heart slices: correlation with established in vitro and in vivo models. *British Journal of Pharmacology*, 166(1), 276–296, doi:[10.1111/j.1476-5381.2011.01775.x](https://doi.org/10.1111/j.1476-5381.2011.01775.x). 19, 20
- Hodgkin, A. L. & Huxley, A. F. (1952). A quantitative description of membrane current and its application to conduction and excitation in nerve. *The Journal of Physiology*, 117(4), 500–544, doi:[10.1113/jphysiol.1952.sp004764](https://doi.org/10.1113/jphysiol.1952.sp004764). 4
- Iyer, V., Mazhari, R., & Winslow, R. L. (2004). A Computational Model of the Human Left-Ventricular Epicardial Myocyte. *Biophysical Journal*, 87(3), 1507–1525, doi:[10.1529/biophysj.104.043299](https://doi.org/10.1529/biophysj.104.043299). 2
- Johnstone, R. H., et al. (2016). Uncertainty and variability in models of the cardiac action potential: Can we build trustworthy models? *Journal of Molecular and Cellular Cardiology*, 96, 49–62, doi:[10.1016/j.yjmcc.2015.11.018](https://doi.org/10.1016/j.yjmcc.2015.11.018). 3
- Keener, J. & Sneyd, J., Eds. (2009). *Mathematical Physiology*. Springer New York. 11
- Kuehn, C. (2015). *Multiple Time Scale Dynamics*. Springer International Publishing. 6
- Lachaud, Q., Aziz, M., Burton, F., MacQuaide, N., Myles, R., Simitev, R., & Smith, G. (2022). Electrophysiological heterogeneity in large populations of rabbit ventricular cardiomyocytes. *Cardiovascular Research*, doi:[10.1093/cvr/cvab375](https://doi.org/10.1093/cvr/cvab375). 2, 3, 4, 9, 10, 12, 13, 14, 15, 16, 18, 19, 20, 21
- Lachaud, Q., MacQuaide, N., Burton, F., & Smith, G. (2018). High-throughput Study of Rabbit Ventricle Action Potential Populations in MI Model. *Biophysical Journal*, 114(3), 625a, doi:[10.1016/j.bpj.2017.11.3377](https://doi.org/10.1016/j.bpj.2017.11.3377). 2
- Li, Z., et al. (2017). Improving the In Silico Assessment of Proarrhythmia Risk by Combining hERG (Human Ether-à-go-go-Related Gene) Channel–Drug Binding Kinetics and Multichannel Pharmacology. *Circulation: Arrhythmia and Electrophysiology*, 10(2), doi:[10.1161/circep.116.004628](https://doi.org/10.1161/circep.116.004628). 10
- McKean, H. (1970). Nagumo's equation. *Advances in Mathematics*, 4(3), 209–223, doi:[10.1016/0001-8708\(70\)90023-x](https://doi.org/10.1016/0001-8708(70)90023-x). 3, 4, 8, 20
- Miller, A. K., et al. (2010). An overview of the CellML API and its implementation. *BMC Bioinformatics*, 11(1), doi:[10.1186/1471-2105-11-178](https://doi.org/10.1186/1471-2105-11-178). 2
- Mirams, G. R., et al. (2011). Simulation of multiple ion channel block provides improved early prediction of compounds' clinical torsadogenic risk. *Cardiovascular Research*, 91(1), 53–61, doi:[10.1093/cvr/cvr044](https://doi.org/10.1093/cvr/cvr044). 11
- Mitchell, C. (2003). A two-current model for the dynamics of cardiac membrane. *Bulletin of Mathematical Biology*, 65(5), 767–793, doi:[10.1016/s0092-8240\(03\)00041-7](https://doi.org/10.1016/s0092-8240(03)00041-7). 3
- Mullen, K. M. (2014). Continuous Global Optimization in R. *Journal of Statistical Software*, 60(6), doi:[10.18637/jss.v060.i06](https://doi.org/10.18637/jss.v060.i06). 13
- Müllenbroich, M. C., et al. (2021). Novel Optics-Based Approaches for Cardiac Electrophysiology: A Review. *Frontiers in Physiology*, 12, doi:[10.3389/fphys.2021.769586](https://doi.org/10.3389/fphys.2021.769586). 2
- Muszkiewicz, A., et al. (2016). Variability in cardiac electrophysiology: Using experimentally-calibrated populations of models to move beyond the single virtual physiological human paradigm. *Progress in Biophysics and Molecular Biology*, 120(1-3), 115–127, doi:[10.1016/j.pbiomolbio.2015.12.002](https://doi.org/10.1016/j.pbiomolbio.2015.12.002). 2, 3
- Nagumo, J., Arimoto, S., & Yoshizawa, S. (1962). An Active Pulse Transmission Line Simulating Nerve Axon. *Proceedings of the IRE*, 50(10), 2061–2070, doi:[10.1109/jrproc.1962.288235](https://doi.org/10.1109/jrproc.1962.288235). 3, 4
- Niederer, S. A., Fink, M., Noble, D., & Smith, N. P. (2009). A meta-analysis of car-

- diac electrophysiology computational models. *Experimental Physiology*, 94(5), 486–495, doi:[10.1113/expphysiol.2008.044610](https://doi.org/10.1113/expphysiol.2008.044610). 2
- Pandit, S. V. (2018). Ionic Mechanisms of Atrial Action Potentials. In *Cardiac Electrophysiology: From Cell to Bedside* (pp. 293–303). Elsevier. 2
- Pontryagin, L. S. (1957). The asymptotic behaviour of systems of differential equations with a small parameter multiplying the highest derivatives. *Izv. Akad. Nauk SSSR, Ser. Mat.*, 21(5), 107–155. 6
- Pouranbarani, E., dos Santos, R. W., & Nygren, A. (2019). A robust multi-objective optimization framework to capture both cellular and intercellular properties in cardiac cellular model tuning: Analyzing different regions of membrane resistance profile in parameter fitting. *PLOS ONE*, 14(11), e0225245, doi:[10.1371/journal.pone.0225245](https://doi.org/10.1371/journal.pone.0225245). 3
- Powell, M. J. D. (1970). A Hybrid Method for Nonlinear Equations. In P. Rabinowitz (Ed.), *Numerical Methods for Nonlinear Algebraic Equations*. Gordon and Breach. 12
- Qu, Z., Hu, G., Garfinkel, A., & Weiss, J. N. (2014). Nonlinear and stochastic dynamics in the heart. *Physics Reports*, 543(2), 61–162, doi:[10.1016/j.physrep.2014.05.002](https://doi.org/10.1016/j.physrep.2014.05.002). 6, 8
- Rinzel, J. & Keller, J. B. (1973). Traveling Wave Solutions of a Nerve Conduction Equation. *Biophysical Journal*, 13(12), 1313–1337, doi:[10.1016/s0006-3495\(73\)86065-5](https://doi.org/10.1016/s0006-3495(73)86065-5). 4
- Sarkar, A. X. & Sobie, E. A. (2010). Regression Analysis for Constraining Free Parameters in Electrophysiological Models of Cardiac Cells. *PLoS Computational Biology*, 6(9), e1000914, doi:[10.1371/journal.pcbi.1000914](https://doi.org/10.1371/journal.pcbi.1000914). 3
- Shannon, T. R., Wang, F., Puglisi, J., Weber, C., & Bers, D. M. (2004). A Mathematical Treatment of Integrated Ca Dynamics within the Ventricular Myocyte. *Biophysical Journal*, 87(5), 3351–3371, doi:[10.1529/biophysj.104.047449](https://doi.org/10.1529/biophysj.104.047449). 2
- Sigg, D. C., Iaizzo, P. A., Xiao, Y.-F., & He, B., Eds. (2010). *Cardiac Electrophysiology Methods and Models*. Springer US. 2
- Simitev, R. D. & Biktashev, V. N. (2011). Asymptotics of Conduction Velocity Restitution in Models of Electrical Excitation in the Heart. *Bulletin of Mathematical Biology*, 73(1), 72–115, doi:[10.1007/s11538-010-9523-6](https://doi.org/10.1007/s11538-010-9523-6). 21
- Sobie, E. A. (2009). Parameter Sensitivity Analysis in Electrophysiological Models Using Multivariable Regression. *Biophysical Journal*, 96(4), 1264–1274, doi:[10.1016/j.bpj.2008.10.056](https://doi.org/10.1016/j.bpj.2008.10.056). 3
- ten Tusscher, K. H. W. J., Noble, D., Noble, P. J., & Panfilov, A. V. (2004). A model for human ventricular tissue. *American Journal of Physiology-Heart and Circulatory Physiology*, 286(4), H1573–H1589, doi:[10.1152/ajpheart.00794.2003](https://doi.org/10.1152/ajpheart.00794.2003). 2
- Tikhonov, A. N. (1952). Systems of Differential Equations, Containing Small Parameters at the Derivatives. *Mat. Sbornik*, 31(3), 575–586. 6, 20
- Tonnellier, A. (2003). The McKean's Caricature of the Fitzhugh–Nagumo Model I. The Space-Clamped System. *SIAM Journal on Applied Mathematics*, 63(2), 459–484, doi:[10.1137/s0036139901393500](https://doi.org/10.1137/s0036139901393500). 4
- Trayanova, N. A., Popescu, D. M., & Shade, J. K. (2021). Machine Learning in Arrhythmia and Electrophysiology. *Circulation Research*, 128(4), 544–566, doi:[10.1161/circresaha.120.317872](https://doi.org/10.1161/circresaha.120.317872). 3
- Tsallis, C. & Stariolo, D. A. (1996). Generalized simulated annealing. *Physica A*, 233(1-2), 395–406, doi:[10.1016/s0378-4371\(96\)00271-3](https://doi.org/10.1016/s0378-4371(96)00271-3). 13
- Tse, G. (2016). Mechanisms of cardiac arrhythmias. *Journal of Arrhythmia*, 32(2), 75–81,



- doi:[10.1016/j.joa.2015.11.003](https://doi.org/10.1016/j.joa.2015.11.003). 1
- Virtanen, P., et al. (2020). SciPy 1.0: Fundamental algorithms for scientific computing in Python. *Nature Methods*, 17, 261–272, doi:[10.1038/s41592-019-0686-2](https://doi.org/10.1038/s41592-019-0686-2). 12, 13
- Wang, W.-P. (1988a). Multiple impulse solutions to McKean's caricature of the nerve equation. I—existence. *Communications on Pure and Applied Mathematics*, 41(1), 71–103, doi:[10.1002/cpa.3160410106](https://doi.org/10.1002/cpa.3160410106). 4
- Wang, W.-P. (1988b). Multiple impulse solutions to McKean's caricature of the nerve equation. II. Stability. *Communications on Pure and Applied Mathematics*, 41(8), 997–1025, doi:[10.1002/cpa.3160410802](https://doi.org/10.1002/cpa.3160410802). 4
- Warren, M., et al. (2010). High-precision recording of the action potential in isolated cardiomyocytes using the near-infrared fluorescent dye di-4-ANBDQBS. *American Journal of Physiology-Heart and Circulatory Physiology*, 299(4), H1271–H1281, doi:[10.1152/ajpheart.00248.2010](https://doi.org/10.1152/ajpheart.00248.2010). 2
- Whittaker, D. G., Clerx, M., Lei, C. L., Christini, D. J., & Mirams, G. R. (2020). Calibration of ionic and cellular cardiac electrophysiology models. *Wiley Interdisciplinary Reviews: Systems Biology and Medicine*, 12(4), e1482, doi:[10.1002/wsbm.1482](https://doi.org/10.1002/wsbm.1482). 3
- Wilhelms, M., Hettmann, H., Maleckar, M. M., Koivumäki, J. T., Dössel, O., & Seemann, G. (2013). Benchmarking electrophysiological models of human atrial myocytes. *Frontiers in Physiology*, 3, doi:[10.3389/fphys.2012.00487](https://doi.org/10.3389/fphys.2012.00487). 3
- Xiang, Y. & Gong, X. G. (2000). Efficiency of generalized simulated annealing. *Physical Review E*, 62(3), 4473–4476, doi:[10.1103/physreve.62.4473](https://doi.org/10.1103/physreve.62.4473). 13